

Towards superresolution surface metrology: Quantum estimation of angular and axial separations

Carmine Napoli,^{1,2,*} Tommaso Tufarelli,^{1,†} Samanta Piano,^{2,‡} Richard K. Leach,^{2,§} and Gerardo Adesso^{1,¶}

¹*School of Mathematical Sciences and Centre for the Mathematics and Theoretical Physics of Quantum Non-Equilibrium Systems, University of Nottingham, University Park Campus, Nottingham NG7 2RD, United Kingdom*

²*Manufacturing Metrology Team, Faculty of Engineering, University of Nottingham, Jubilee Campus, Nottingham NG8 1BB, United Kingdom*

(Dated: May 17, 2022)

We investigate localization of two incoherent point sources with arbitrary angular and axial separations in the paraxial approximation. By using quantum metrology techniques, we show that a simultaneous estimation of the two separations and of the two corresponding coordinates of the centroid is achievable by a single quantum measurement, with a precision saturating the ultimate limit stemming from the quantum Cramér-Rao bound. Such a precision is not degraded in the sub-wavelength regime, thus overcoming the traditional limitations of classical direct imaging derived from Rayleigh's criterion. Our results are qualitatively independent of the point spread function of the imaging system, and quantitatively illustrated in detail for the Gaussian instance. This analysis may have relevant applications in three-dimensional surface measurements.

Introduction.— High-resolution imaging is a cornerstone of modern science and engineering, which has enabled revolutionary advances in astronomy, manufacturing, biochemistry, and medical diagnostics. In traditional direct imaging based on classical wave optics, two incoherent point sources with angular separation smaller than the wavelength of the emitted light cannot be resolved due to fundamental diffraction effects [1], a phenomenon recently dubbed “Rayleigh’s curse” [2]. Several techniques, including most prominently fluorescence microscopy [3], have been introduced in recent years to overcome this limitation and achieve sub-wavelength imaging [4, 5]. Nevertheless, to determine the ultimate limits of optical resolution one needs to resort to a full quantum mechanical description of the imaging process [6]. In this respect, a breakthrough has been reported in a series of works [2, 7–17] initiated by Tsang and collaborators [2], who employed techniques from quantum metrology [18–21] to prove that the achievable error in estimating the angular separation of two incoherent point sources, in the paraxial approximation, is in fact independent of said separation (no matter how small), provided an optimal detection scheme is performed on the image plane. These results, which stem from the fundamental quantum Cramér-Rao bound [18, 19] and *de facto* banish Rayleigh’s curse [2], have been corroborated by proof-of-principle experiments [22–25].

The studies presented so far on quantum superlocalization, however, were limited to the case of point sources aligned on the same object plane, thus neglecting their axial separation. The optical lateral resolution of an imaging system is an important characteristic but its usefulness can be misleading when considering the measurement of non-flat surfaces [26]. When probing surface topography, the spacing of the points in an image must be considered, along with the ability to accurately determine the heights of features. In other words, the lateral resolution must be considered in conjunction with the ability of the system to transfer surface amplitudes [27].

To address this issue, here we consider the simultaneous estimation of both angular and axial separations, as well as the corresponding centroid coordinates, of two incoherent point

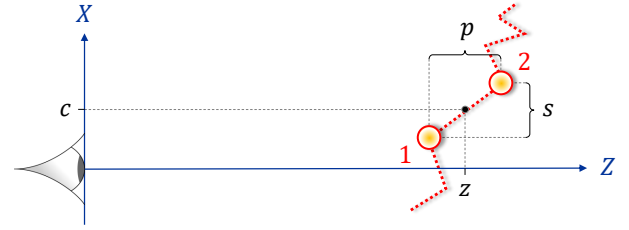


Figure 1. Schematic of the two incoherent sources. The four parameters to be estimated are: the angular separation s , the axial separation p , the angular centroid coordinate c , and the axial centroid coordinate z .

sources aligned in general on different object planes. These point sources may model, e.g., two emitters at the edges of a steep section on a rough surface, as indicated by the red dotted outline in Figure 1.

We tackle the problem by resorting to the toolbox of *multi-parameter quantum metrology*, a branch of quantum technology which is attracting increasing interest thanks to its prominent role in fundamental science and applications [18–21, 28–49]. We find that Rayleigh’s curse does not occur even when the sources have a nonzero axial separation, and all four unknown parameters can be estimated simultaneously by means of a single optimal quantum measurement, meeting the compatibility requirements for saturation of the multiparameter quantum Cramér-Rao bound [28, 31]. These results are independent of the point spread function of the imaging system. We then specialise to the illustrative case of a Gaussian point spread function, and derive analytical formulas for the achievable estimation error and its scaling with the parameters of interest as determined by the quantum Fisher information matrix, showing that in the limit of small angular and axial distances all the parameters become statistically independent.

Sources and imaging system model.— We approach the problem of estimating both axial and angular separation of two point sources by following a similar approach to Ref. [2], which is in turn inspired by Rayleigh’s work [1]. We assume that the detectable light on the image plane can be described

as an incoherent superposition of two quasi-monochromatic scalar paraxial waves, one coming from each source. As shown in Figure 1, our two sources are in general not lying on the same object plane (an ‘object plane’ is a plane perpendicular to the optical axis Z), and they feature an angular separation s and an axial separation p .

Considering thermal sources at optical frequencies, we divide the total emission time into short coherence time intervals τ_c , so that within each interval the sources can be assumed weak, i.e., effectively emitting at most one photon. This is a standard approach for modelling incoherent thermal sources [50–56], and it allows us to describe the quantum state ρ of the optical field on the image plane as a mixture of a zero-photon state ρ_0 and a one-photon state ρ_1 in each time interval (neglecting contributions from higher photon numbers) [57],

$$\rho = (1 - \varepsilon)\rho_0 + \varepsilon\rho_1 + o(\varepsilon^2), \quad (1)$$

where $\varepsilon \ll 1$ is the average number of photons impinging on the image plane. In practice, a detectable signal is obtained by measuring the optical field for a time $t \gg \tau_c$, so that many coherence time intervals are included, resulting in a non-negligible mean photon number.

Inspired by the expression for the electric field amplitude of a Gaussian beam [58], we assume that the image-plane field amplitude generated by each source takes the form

$$\Psi_{\vec{R}_r}(x) \equiv \exp[-ikZ_r]\psi_{Z_r}(x - X_r), \quad (2)$$

where x is the image-plane coordinate, $\vec{R}_r = (X_r, Z_r)$ are the coordinates of the sources $r = 1, 2$, X_r being the coordinate perpendicular to the optical axis and Z_r the axial distance to the image plane. We are assuming a shift-invariant imaging system, and in the spirit of the paraxial approximation the functions ψ_{Z_r} are assumed real, so that the phase of each field amplitude $\Psi_{\vec{R}_r}(x)$ is entirely determined by the factor $\exp[-ikZ_r]$, where k is the (average) wave number of the emitted light [59]. We shall indicate with $a(x)$ the field annihilation operator at position x on the image plane, satisfying the bosonic commutation rule $[a(x), a^\dagger(x')] = \delta(x - x')$.

We can then write the imaging system field state, corresponding to the emission of one photon by source r , as

$$|\Psi_{\vec{R}_r}\rangle = e^{-ikZ_r} \int_{-\infty}^{+\infty} \psi_{Z_r}(x - X_r) a^\dagger(x) |0\rangle dx, \quad (3)$$

where $|0\rangle$ is the field vacuum state.

Multiparameter estimation and quantum Cramér-Rao bound.— We work under the assumption that the photon statistics of our sources is Poissonian, following a similar approach as in Ref. [2]. We can thus assume that in a single run of the experiment, which lasts for M coherence time intervals, M copies of the state ρ in Eq. (1) are prepared and measured (equivalently, one may consider the input state $\rho^{\otimes M}$). On average, this yields $M\varepsilon$ photons per run. In order to apply the standard tools of estimation theory, we further assume that $\nu \gg 1$ runs are performed, after which the measurement data are processed to build estimators for the unknown parameters.

In our case, the parameters of interest are the angular and axial relative coordinates and the centroid coordinates of the sources, indicated as s, c, p, z , see Figure 1. We thus write the state ρ as a function of four parameters $\{\lambda_\mu\}_{\mu=1,\dots,4}$, where

$$\begin{aligned} \lambda_1 \equiv s &= X_2 - X_1, & \lambda_2 \equiv c &= \frac{X_2 + X_1}{2}, \\ \lambda_3 \equiv p &= Z_2 - Z_1, & \lambda_4 \equiv z &= \frac{Z_2 + Z_1}{2}, \end{aligned} \quad (4)$$

The statistical error (variance) $\Delta\lambda_\mu^2$ of any *unbiased* estimator of the unknown parameter λ_μ is lower bounded via the quantum Cramér-Rao bound (qCRb) [18, 19]

$$\sum_{\mu=1}^4 \Delta\lambda_\mu^2 \geq \frac{1}{\nu M \varepsilon} \text{Tr}[H^{-1}], \quad (5)$$

where H is the quantum Fisher information matrix (qFim) of the single-photon state ρ_1 (equivalently, this can be seen as the qFim per coherence time interval per photon). The prefactor on the RHS of Eq. (5) is obtained by exploiting the additivity property $\text{qFim}(\rho^{\otimes M}) = M \times \text{qFim}(\rho)$, and by noting that $\text{qFim}(\rho) \simeq \varepsilon \times \text{qFim}(\rho_1)$ at leading order in ε (since the field vacuum state ρ_0 is independent of all source parameters). The resulting linear dependence on the total photon number $\nu M \varepsilon$ is characteristic of classical light sources [21, 60].

The qCRb suggests that, the higher the qFim element $H_{\mu\mu}$, the more precisely (i.e., with lower statistical error) one may be able to estimate the parameter λ_μ , by performing a suitable measurement. While for a single parameter the qCRb can always be saturated asymptotically by means of an adaptive procedure [20], this is no longer the case for multiparameter estimation, as the parameters may not always be compatible [31]; we will discuss this issue in detail later in the manuscript.

Results.— We recall that the qFim elements are given by

$$H_{\mu\nu} = \text{Re} \left[\text{Tr}(\rho_1 L_\mu L_\nu) \right], \quad (6)$$

where L_μ is the symmetric logarithmic derivative for the parameter λ_μ , defined implicitly by the equation

$$2 \frac{\partial \rho_1}{\partial \lambda_\mu} = L_\mu \rho_1 + \rho_1 L_\mu. \quad (7)$$

The analytical computation of H is presented in detail in Appendix A and it relies on the expansion of ρ_1 and its derivatives on an appropriate orthonormal basis, followed by standard linear algebraic manipulations. While still tedious, the calculation is simplified by the factorization of the field generated by each source into a real point spread function ψ_{Z_r} times an x -independent phase factor $\exp[-ikZ_r]$, as indicated in Eq. (2). Following this model, we find that the qFim is composed of

the diagonal elements

$$\begin{aligned}
H_{ss} &= \frac{1}{2} (\Delta X_1^2 + \Delta X_2^2), \\
H_{cc} &= 2 (\Delta X_1^2 + \Delta X_2^2 - 2\gamma^2), \\
H_{pp} &= \frac{1}{4(1-\delta^2)} \left\{ 2(\Delta Z_1^2 + \Delta Z_2^2)(1-\delta^2) \right. \\
&\quad \left. - (\Gamma_{12} + \Gamma_{21})^2 - 4\Gamma_{21}\delta(\delta_{Z_1} + \delta_{Z_2}) \right. \\
&\quad \left. + ((\Gamma_{12} + \Gamma_{21})\delta + (\Delta Z_1^2 + \Delta Z_2^2))^2 \right\}, \\
H_{zz} &= \frac{1}{1-\delta^2} \left\{ 2(\Delta Z_1^2 + \Delta Z_2^2)(1-\delta^2) \right. \\
&\quad \left. - (\Gamma_{12} - \Gamma_{21})^2(1-\delta^2) - (\Gamma_{12} + \Gamma_{21})^2 \right. \\
&\quad \left. + ((\delta_{Z_1} + \delta_{Z_2}) - \Gamma_{12} - \Gamma_{21})^2 \right\};
\end{aligned} \tag{8}$$

while the off-diagonal elements are

$$\begin{aligned}
H_{sc} &= -(\Delta Z_1^2 - \Delta Z_2^2), \\
H_{sp} &= \frac{(\delta_{Z_1} + \delta_{Z_2})\gamma\delta}{2(1-\delta^2)}, \quad H_{sz} = \frac{(\delta_{Z_1} + \delta_{Z_2})\gamma}{2(1-\delta^2)}, \\
H_{cp} &= (\Gamma_{12} + \Gamma_{21})\gamma, \quad H_{cz} = -2(\Gamma_{12} - \Gamma_{21})\gamma, \\
H_{pz} &= -\frac{1}{2(1-\delta^2)} \left\{ 2(\Delta Z_1^2 + \Delta Z_2^2)(1-\delta^2) \right. \\
&\quad \left. - (\Gamma_{12}^2 - \Gamma_{21}^2)(1-\delta^2) - \delta(\delta_{Z_1} + \delta_{Z_2})^2 \right. \\
&\quad \left. - (\Gamma_{12}(1-\delta) - \Gamma_{21}(1+\delta))(\delta_{Z_1} + \delta_{Z_2}) \right\},
\end{aligned} \tag{9}$$

where

$$\begin{aligned}
\delta &= \int_{-\infty}^{+\infty} \psi_{Z_1}(x - X_1) \psi_{Z_2}(x - X_2) dx, \\
\Delta X_r^2 &= \int_{-\infty}^{\infty} \left[\frac{\partial \psi_{Z_r}(x - X_r)}{\partial X_r} \right]^2 dx, \\
\Delta Z_r^2 &= \int_{-\infty}^{\infty} \left[\frac{\partial \psi_{Z_r}(x - X_r)}{\partial Z_r} \right]^2 dx, \\
\gamma &= \int_{-\infty}^{\infty} \left[\frac{\partial \psi_{Z_r}(x)}{\partial x} \right] \psi_{Z_r}(x - s) dx, \\
\Gamma_{12} &= \int_{-\infty}^{\infty} \left[\frac{\partial \psi_{Z_1}(x - X_1)}{\partial Z_1} \right] \psi_{Z_2}(x - X_2) dx, \\
\Gamma_{21} &= \int_{-\infty}^{\infty} \left[\frac{\partial \psi_{Z_2}(x - X_2)}{\partial Z_2} \right] \psi_{Z_1}(x - X_1) dx, \\
\delta_{X_r} &= \frac{\partial \delta}{\partial X_r}, \quad \delta_{Z_r} = \frac{\partial \delta}{\partial Z_r},
\end{aligned}$$

are functions of the unknown parameters s , c , p and z .

While the above formulas are valid for an arbitrary form of the point spread function, in order to provide a concrete example we specialise in what follows to the Gaussian case,

$$\psi_{Z_r}(x) = (4\pi\sigma^2(Z_r))^{-1/4} \exp[-x^2/4\sigma^2(Z_r)], \tag{10}$$

where we are assuming $\sigma^2(Z_r) = \sigma_0 Z_r/z$, i.e. the width of the point spread function scales linearly with the axial distance Z_r , and σ_0 is a reference width parameter. Eq. (10) can be obtained, for example, if the fields generated by the two sources

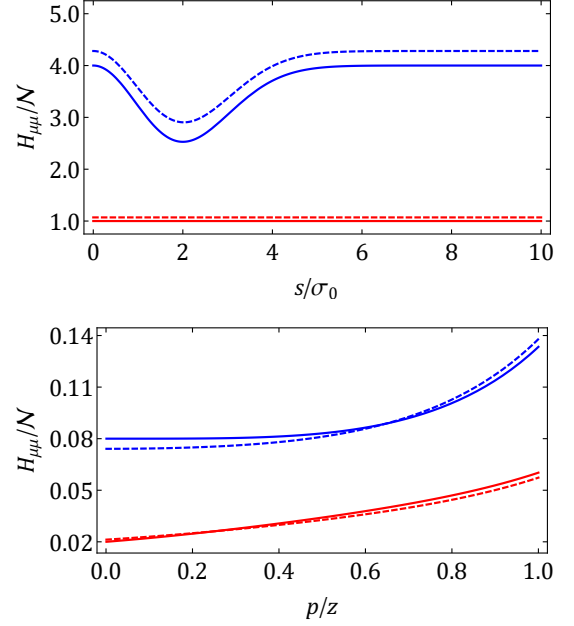


Figure 2. **Top: Angular localization.** Plots of the qFim elements H_{ss} (red, lowermost curves) and H_{cc} (blue, uppermost curves), versus the angular separation s normalized by the reference width σ_0 of a Gaussian point spread function [see Eq. (10)]; continuous lines refer to $p = 0$ and dashed lines to $p/z = 0.3$. **Bottom: Axial localization.** Plots of the qFim elements H_{pp} (red, lowermost curves) and H_{zz} (blue, uppermost curves), versus the axial separation p normalized by the axial centroid coordinate z ; continuous lines are for $s = 0$ and dashed lines for $s/\sigma_0 = 0.8$. The vertical axis in both panels is normalized so that $H_{ss} = 1$ when $p = 0$.

are well approximated by Gaussian beams in the vicinity of the image plane [58]. By utilizing Eq. (10) in the calculations of the qFim elements, we find formulas that are fully analytical (albeit too cumbersome to be reported explicitly here without further approximations) and allow us to perform a comprehensive analysis of the multi-parameter estimation problem under investigation. Furthermore, the Gaussian case bears the advantage that it can be easily compared with the existing literature that tackled the estimation of s alone (typically fixing $p = 0$). To support the solidity of our results, we have indeed checked that, in the limit $p \rightarrow 0$, our expression for H_{ss} matches the appropriate quantities in Refs. [2, 60].

Figure 2 exemplifies how our results provide new insights on the problem of sub-wavelength imaging, while correctly reproducing what is known for $p = 0$ — compare e.g. the top panel with Fig. 2 in Ref. [2]. We note in particular that H_{ss} stays independent of s also when $p \neq 0$, which means that Rayleigh's curse does not affect the estimation of the angular separation s even for two sources with nonzero axial separation p . In fact, having a nonzero p improves the estimation of the angular separation s and centroid coordinate z , as indicated by the increase of the corresponding qFim elements. Interestingly, our results become particularly transparent in the regime $\frac{p}{z} \ll 1$ and $ks \ll 1$, which is precisely the one of rel-

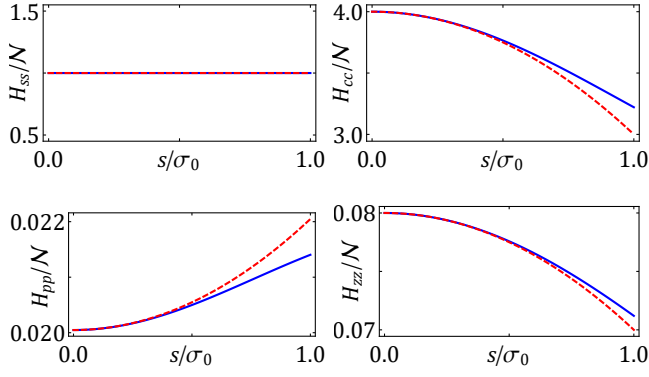


Figure 3. Plots of the diagonal qFim elements for the angular and axial distances and centroid coordinates versus the angular separation for a Gaussian point spread function. The continuous (blue) line corresponds to the exact analytical results, while the dashed (red) line to the approximations for $p/z \ll 1$ and $ks \ll 1$ as given in Eq. (11).

evance to sub-wavelength imaging: at leading order in these small terms, the qFim simplifies as

$$H \approx \begin{pmatrix} \left(1 + \frac{3p^2}{4z^2}\right)\mathcal{N} & \frac{2p}{z}\mathcal{N} & \frac{s}{2z}\mathcal{N} & \frac{s}{z}\mathcal{N} \\ \frac{2p}{z}\mathcal{N} & 4\mathcal{N}\left(1 + \frac{3p^2}{4z^2} - s^2\mathcal{N}\right) & 0 & -\frac{2ps}{z^2}\mathcal{N} \\ \frac{s}{2z}\mathcal{N} & 0 & \frac{1 + \frac{p^2}{z^2} + \frac{p}{z} + \frac{s^2\mathcal{N}}{2}}{2z^2} & -\frac{p}{2z^3} \\ \frac{s}{z}\mathcal{N} & -\frac{2ps}{z^2}\mathcal{N} & -\frac{p}{2z^3} & \frac{2 - s^2\mathcal{N}}{z^2} \end{pmatrix}, \quad (11)$$

where $\mathcal{N} = \frac{k^2\sigma_0^2}{16z^2}$ is a normalization factor.

Taking advantage of the above approximate formula, we can now move on to investigate the actual precision with which our parameters of interest can be determined, and how close we can get to the limits imposed by the qCRb in practical experiments. In quantum estimation theory, multiparameter problems embody a nontrivial generalization of the single-parameter case [20, 28, 30, 31]: if an estimation scheme is optimized for a particular parameter, it typically results into an increased error in estimating the others. However, in the best case scenario, such a trade-off does not apply, and one can identify an optimal protocol for the estimation of all the parameters simultaneously. This happens if and only if the parameters are *compatible*, i.e., they satisfy the following conditions [31]: (i) There is a single probe state yielding the maximal qFim element for each of the parameters; (ii) There is a single measurement which is jointly optimal for extracting information on all the parameters from the output state, ensuring the asymptotic saturability of the qCRb; (iii) The parameters are statistically independent, meaning that the indeterminacy of one of them does not affect the error on estimating the others. We recall also that (ii) holds iff $\text{Tr}(\rho_1[L_\mu, L_\nu]) = 0 \quad \forall \mu \neq \nu$, while (iii) is equivalent to the condition $H_{\mu\nu} = 0 \quad \forall \mu \neq \nu$.

In this paper we do not focus on the first condition, since our theory is built around a realistic imaging scenario in which the emission properties of the sources are fixed in advance. Yet, it

is worth investigating conditions (ii) and (iii), since they have crucial implications for the actual achievability of the statistical errors given by the qCRb. Remarkably, we find that condition (ii) is *always satisfied* in the problem under consideration — independently of the specifics of the point spread function (See Appendix B) — so that it is possible to construct a physical measurement and estimation strategy saturating Eq. (5) asymptotically [28, 31].

On the other hand, condition (iii) does not hold in general. However, as we can see in Eq. (11) for the Gaussian model, the off-diagonal elements of the qFim depend linearly on s and p , therefore when $s \approx 0$ and $p \approx 0$ the qFim becomes

$$H \approx \text{diag} \left\{ \frac{k^2\sigma_0^2}{16z^2}, \frac{k^2\sigma_0^2}{4z^2}, \frac{1}{2z^2}, \frac{1}{z^2} \right\}, \quad (12)$$

meaning that the four parameters s, c, p, z are approximately statistically independent when the two sources have infinitesimal angular and axial separation. The behaviour of the qFim elements for all four parameters as a function of the angular distance is illustrated in Figure 3. From the plots and from Eq. (12), we see that the qFim diagonal elements tend to a nonzero value when $s, p \rightarrow 0$, meaning that the total estimation error $\propto \text{Tr}[H^{-1}]$ achievable by the optimal quantum procedure stays finite even when the two sources are infinitesimally close, instead of diverging as in direct imaging [1, 2].

Conclusions.— We determined the ultimate quantum limits to the simultaneous estimation of both angular and axial separations and centroid coordinates of two incoherent point sources on different object planes in the paraxial approximation. Our results indicate that there exists a jointly optimal detection scheme that enables resolving the sources even when arbitrarily close, reasserting that Rayleigh’s curse is merely an artefact of classical detection in direct imaging. In practice, a measurement apparatus approaching the optimal precision can be designed by adapting the methods of [15, 16, 45], in particular extending the “spatial-mode demultiplexing” or “superlocalization by image inversion interferometry” techniques [2, 7] to the axially separated setting considered here.

While some of our findings were illustrated explicitly for Gaussian beams, our framework is general and can be applied to calculate the achievable metrological precision in other relevant cases (such as a Jinc point spread function, resulting from a circular aperture), thanks to the exact expressions in Eqs. (8,9). This leads to qualitatively similar results as those presented here. In particular, the two most important conclusions, namely that the quantum Fisher information for the angular distance s is independent of s even for a nonzero axial distance p , and that the joint estimation of s, c, p, z fulfils the measurement compatibility condition leading to the saturation of the quantum Cramér-Rao bound in Eq. (5), are in fact valid for any point spread function.

This work constitutes an important application of multiparameter quantum estimation theory to a realistic imaging setting, extending the seminal work of Ref. [2]. Our analysis, combined with the one in [12], yields a quantum enhanced toolbox for full 3D sub-wavelength localization. This paves

the way to further experimental demonstrations and innovative metrology solutions in scientific, industrial and biomedical domains, such as sub-nanometre depth mapping in rough surfaces, and dynamical interaction analysis of heterogeneous molecules in a cellular environment [4, 5, 26, 61].

Acknowledgments.— We thank M. Barbieri, D. Braun, M. Guta, H. Harmon, M. Khalifa, P. Knott, I. Lesanovsky, P. Liuzzo-Scorpo, C. Lupo, R. Nair, R. Nichols, M. Pezzali, S. Pirandola, S. Ragy, R. Su, N. Treps, M. Tsang, and J.-P. Wolf for useful discussions. This work was supported by the European Research Council under the Starting Grant GQCOP (Grant No. 637352), the Royal Society under the International Exchanges Programme (Grant No. IE150570), the EPSRC under a Manufacturing Fellowship (Grant No. EP/M008983/1), the University of Nottingham under a Nottingham Research Fellowship and a FROG Scholarship, and the EPSRC DTG Centre in Complex Systems and Processes.

* carmine.napoli@nottingham.ac.uk

† tommaso.tufarelli@nottingham.ac.uk

‡ samanta.piano@nottingham.ac.uk

§ richard.leach@nottingham.ac.uk

¶ gerardo.adesso@nottingham.ac.uk

- [1] L. Rayleigh, “Xxxi. investigations in optics, with special reference to the spectroscope,” *The London, Edinburgh, and Dublin Philosophical Magazine and Journal of Science* **8**, 261 (1879).
- [2] M. Tsang, R. Nair, and X.-M. Lu, “Quantum theory of super-resolution for two incoherent optical point sources,” *Physical Review X* **6**, 031033 (2016).
- [3] L. Möckl, D. C. Lamb, and C. Bruchle, “Super-resolved Fluorescence Microscopy: Nobel Prize in Chemistry 2014 for Eric Betzig, Stefan Hell, and William E. Moerner,” *Angewandte Chemie International Edition* **53**, 13972.
- [4] W. E. Moerner, “New directions in single-molecule imaging and analysis,” *Proceedings of the National Academy of Sciences* **104**, 12596 (2007), <http://www.pnas.org/content/104/31/12596.full.pdf>.
- [5] R. K. Leach and B. Sherlock, “Applications of super-resolution imaging in the field of surface topography measurement,” *Surface Topography: Metrology and Properties* **2**, 023001 (2014).
- [6] M. Genovese, “Real applications of quantum imaging,” *Journal of Optics* **18**, 073002 (2016).
- [7] R. Nair and M. Tsang, “Interferometric superlocalization of two incoherent optical point sources,” *Optics express* **24**, 3684 (2016).
- [8] R. Nair and M. Tsang, “Far-field superresolution of thermal electromagnetic sources at the quantum limit,” *Physical Review Letters* **117**, 190801 (2016).
- [9] C. Lupo and S. Pirandola, “Ultimate precision bound of quantum and subwavelength imaging,” *Physical Review Letters* **117**, 190802 (2016).
- [10] M. Tsang, “Subdiffraction incoherent optical imaging via spatial-mode demultiplexing,” *New Journal of Physics* **19**, 023054 (2017).
- [11] R. Kerviche, S. Guha, and A. Ashok, “Fundamental limit of resolving two point sources limited by an arbitrary point spread function,” in *Information Theory (ISIT), 2017 IEEE International Symposium on* (IEEE, 2017) pp. 441–445.
- [12] S. Z. Ang, R. Nair, and M. Tsang, “Quantum limit for two-dimensional resolution of two incoherent optical point sources,” *Physical Review A* **95**, 063847 (2017).
- [13] A. Chrostowski, R. Demkowicz-Dobrzański, M. Jarzyna, and K. Banaszek, “On super-resolution imaging as a multiparameter estimation problem,” *International Journal of Quantum Information*, 1740005 (2017).
- [14] J. Řehaček, Z. Hradil, B. Stoklasa, M. Paúr, J. Grover, A. Krzic, and L. Sánchez-Soto, “Multiparameter quantum metrology of incoherent point sources: Towards realistic superresolution,” *Physical Review A* **96**, 062107 (2017).
- [15] J. Řehaček, M. Paúr, B. Stoklasa, Z. Hradil, and L. Sánchez-Soto, “Optimal measurements for resolution beyond the rayleigh limit,” *Optics Letters* **42**, 231 (2017).
- [16] J. Řehaček, Z. Hradil, D. Koutny, J. Grover, A. Krzic, and L. Sánchez-Soto, “Optimal measurements for multiparameter quantum metrology with mixed states,” *arXiv preprint arXiv:1712.08524* (2017).
- [17] S. Zhou and L. Jiang, “A modern description of rayleigh’s criterion,” *arXiv preprint arXiv:1801.02917* (2018).
- [18] C. W. Helstrom, *Quantum Detection and Estimation Theory* (Academic Press, New York, 1976).
- [19] S. L. Braunstein and C. M. Caves, “Statistical distance and the geometry of quantum states,” *Physical Review Letters* **72**, 3439 (1994).
- [20] M. G. A. Paris, “Quantum estimation for quantum technology,” *International Journal of Quantum Information* **07**, 125 (2009).
- [21] V. Giovannetti, S. Lloyd, and L. Maccone, “Advances in quantum metrology,” *Nature Photonics* **5**, 222 (2011).
- [22] F. Yang, A. Tashchilina, E. S. Moiseev, C. Simon, and A. I. Lvovsky, “Far-field linear optical superresolution via heterodyne detection in a higher-order local oscillator mode,” *Optica* **3**, 1148 (2016).
- [23] M. Paúr, B. Stoklasa, Z. Hradil, L. L. Sánchez-Soto, and J. Řehaček, “Achieving the ultimate optical resolution,” *Optica* **3**, 1144 (2016).
- [24] Z. S. Tang, K. Durak, and A. Ling, “Fault-tolerant and finite-error localization for point emitters within the diffraction limit,” in *Frontiers in Optics 2016* (Optical Society of America, 2016) p. FTu2F.6.
- [25] W.-K. Tham, H. Ferretti, and A. M. Steinberg, “Beating rayleigh’s curse by imaging using phase information,” *Physical Review Letters* **118**, 070801 (2017).
- [26] R. K. Leach, C. Evans, L. He, A. Davies, A. Duparr, A. Henning, C. W. Jones, and D. O’Connor, “Open questions in surface topography measurement: a roadmap,” *Surface Topography: Metrology and Properties* **3**, 013001 (2015).
- [27] X. C. De Lega and P. de Groot, “Lateral resolution and instrument transfer function as criteria for selecting surface metrology instruments,” in *Optical Fabrication and Testing* (Optical Society of America, 2012) pp. OTu1D–4.
- [28] K. Matsumoto, “A new approach to the cramér-rao-type bound of the pure-state model,” *Journal of Physics A: Mathematical and General* **35**, 3111 (2002).
- [29] G. Tóth and I. Apellaniz, “Quantum metrology from a quantum information science perspective,” *Journal of Physics A: Mathematical and Theoretical* **47**, 424006 (2014).
- [30] M. Szczykulska, T. Baumgratz, and A. Datta, “Multi-parameter quantum metrology,” *Advances in Physics: X* **1**, 621 (2016).
- [31] S. Ragy, M. Jarzyna, and R. Demkowicz-Dobrzański, “Compatibility in multiparameter quantum metrology,” *Physical Review A* **94**, 052108 (2016).

- [32] D. Braun, G. Adesso, F. Benatti, R. Floreanini, U. Marzolino, M. W. Mitchell, and S. Pirandola, “Quantum enhanced measurements without entanglement,” arXiv preprint arXiv:1701.05152, *Reviews of Modern Physics* (in press) (2018).
- [33] L. Pezzè, A. Smerzi, M. K. Oberthaler, R. Schmied, and P. Treutlein, “Quantum metrology with nonclassical states of atomic ensembles,” arXiv preprint arXiv:1609.01609, *Reviews of Modern Physics* (in press) (2018).
- [34] A. Monras and F. Illuminati, “Measurement of damping and temperature: Precision bounds in gaussian dissipative channels,” *Physical Review A* **83**, 012315 (2011).
- [35] M. Genoni, M. Paris, G. Adesso, H. Nha, P. Knight, and M. Kim, “Optimal estimation of joint parameters in phase space,” *Physical Review A* **87**, 012107 (2013).
- [36] S. Steinlechner, J. Bauchrowitz, M. Meinders, H. Müller-Ebhardt, K. Danzmann, and R. Schnabel, “Quantum-dense metrology,” *Nature Photonics* **7**, 626 (2013).
- [37] O. Pinel, P. Jian, N. Treps, C. Fabre, and D. Braun, “Quantum parameter estimation using general single-mode gaussian states,” *Physical Review A* **88**, 040102 (2013).
- [38] P. C. Humphreys, M. Barbieri, A. Datta, and I. A. Walmsley, “Quantum enhanced multiple phase estimation,” *Physical Review Letters* **111**, 070403 (2013).
- [39] P. J. Crowley, A. Datta, M. Barbieri, and I. A. Walmsley, “Tradeoff in simultaneous quantum-limited phase and loss estimation in interferometry,” *Physical Review A* **89**, 023845 (2014).
- [40] M. D. Vidrighin, G. Donati, M. G. Genoni, X.-M. Jin, W. S. Kolthammer, M. Kim, A. Datta, M. Barbieri, and I. A. Walmsley, “Joint estimation of phase and phase diffusion for quantum metrology,” *Nature Communications* **5**, 3532 (2014).
- [41] L. Banchi, S. L. Braunstein, and S. Pirandola, “Quantum fidelity for arbitrary gaussian states,” *Physical Review Letters* **115**, 260501 (2015).
- [42] T. Baumgratz and A. Datta, “Quantum enhanced estimation of a multidimensional field,” *Physical Review Letters* **116**, 030801 (2016).
- [43] M. Altorio, M. G. Genoni, F. Somma, and M. Barbieri, “Metrology with unknown detectors,” *Physical Review Letters* **116**, 100802 (2016).
- [44] S. Pirandola and C. Lupo, “Ultimate precision of adaptive noise estimation,” *Physical review letters* **118**, 100502 (2017).
- [45] L. Pezzè, M. A. Ciampini, N. Spagnolo, P. C. Humphreys, A. Datta, I. A. Walmsley, M. Barbieri, F. Sciarrino, and A. Smerzi, “Optimal measurements for simultaneous quantum estimation of multiple phases,” *Physical Review Letters* **119**, 130504 (2017).
- [46] R. Yousefjani, R. Nichols, S. Salimi, and G. Adesso, “Estimating phase with a random generator: Strategies and resources in multiparameter quantum metrology,” *Physical Review A* **95**, 062307 (2017).
- [47] R. Nichols, P. Liuzzo-Scorpo, P. A. Knott, and G. Adesso, “Multiparameter gaussian quantum metrology,” arXiv preprint arXiv:1711.09132 (2017).
- [48] T. J. Proctor, P. A. Knott, and J. A. Dunningham, “Multiparameter estimation in networked quantum sensors,” *Physical Review Letters* **120**, 080501 (2018).
- [49] R. Nair, “Quantum-limited loss sensing: Multiparameter estimation and bures distance between loss channels,” arXiv preprint arXiv:1804.02211 (2018).
- [50] A. Labeyrie, S. G. Lipson, and P. Nisenson, *An introduction to optical stellar interferometry* (Cambridge University Press, 2006).
- [51] J. Zmuidzinas, “Cramer-rao sensitivity limits for astronomical instruments: implications for interferometer design,” *JOSA A* **20**, 218 (2003).
- [52] J. W. Goodman, *Statistical optics* (John Wiley & Sons, 2015).
- [53] L. Mandel and E. Wolf, *Optical coherence and quantum optics* (Cambridge University Press, 1995).
- [54] L. Mandel, “Fluctuations of photon beams: the distribution of the photo-electrons,” *Proceedings of the Physical Society* **74**, 233 (1959).
- [55] D. Gottesman, T. Jennewein, and S. Croke, “Longer-baseline telescopes using quantum repeaters,” *Physical Review Letters* **109**, 070503 (2012).
- [56] M. Tsang, “Quantum nonlocality in weak-thermal-light interferometry,” *Physical Review Letters* **107**, 270402 (2011).
- [57] However, the assumption of weak sources can be lifted as in [8, 9], leading to similar qualitative results for thermal sources of arbitrary intensity.
- [58] O. Svelto and D. C. Hanna, *Principles of lasers* (Springer, 1998).
- [59] J. W. Goodman, *Introduction to Fourier optics* (Roberts and Company Publishers, 2005).
- [60] M. Tsang, “Quantum limits to optical point-source localization,” *Optica* **2**, 646 (2015).
- [61] J. Wolf, “Coherent quantum control in biological systems,” in *Biophotonics: Spectroscopy, Imaging, Sensing, and Manipulation* (Springer, 2011) pp. 183–201.

SUPPLEMENTAL MATERIAL

Appendix A: Derivation of the quantum Fisher information matrix

Here we report the derivation of the quantum Fisher information matrix (qFim) H , defined by Eqs. (6) and (7) in the main text, in terms of the symmetric logarithmic derivative (SLD) L_μ for the parameter set $\{\lambda_\mu\}_{\mu=1,\dots,4}$, specified by Eq. (4) in the main text. The general expression reported here is valid for an arbitrary point spread function compliant with the condition given by Eq. (2) in the main text, according to the paraxial approximation.

As mentioned, the vacuum state ρ_0 does not contain any information, while multiple photon emissions are neglected as rare events, therefore the information about the parameters is entirely contained in the one-photon state ρ_1 .

Writing ρ_1 in its eigenbasis,

$$\rho_1 = \sum_i d_i |e_i\rangle \langle e_i|, \quad (S1)$$

then the SLD L_μ can be expressed as

$$L_\mu = \sum_{\substack{i,j \\ d_i+d_j \neq 0}} \frac{2}{d_i+d_j} \langle e_i | \frac{\partial \rho}{\partial \lambda_\mu} | e_j \rangle |e_i\rangle \langle e_j|. \quad (S2)$$

To compute the qFim according to Eqs. (6) and (S2), therefore, we first need to diagonalize the rank-2 state ρ_1 , completing its eigenbasis so that the eigenvectors $\{|e_i\rangle\}$ span the support of $\partial \rho_1 / \partial \lambda_\mu$.

The partial derivative of ρ_1 with respect to λ_μ can be expressed as

$$\frac{\partial \rho_1}{\partial \lambda_\mu} = \frac{\partial}{\partial \lambda_\mu} \sum_i d_i |e_i\rangle \langle e_i| + \sum_i \left[\frac{\partial d_i}{\partial \lambda_\mu} |e_i\rangle \langle e_i| + d_i \frac{\partial |e_i\rangle}{\partial \lambda_\mu} \langle e_i| + d_i |e_i\rangle \frac{\partial \langle e_i|}{\partial \lambda_\mu} \right], \quad (S3)$$

where the support of ρ_1 is spanned by the first two eigenvectors,

$$|e_1\rangle = \frac{|\Psi_{\vec{R}_1}\rangle - e^{-ik(Z_1-Z_2)} |\Psi_{\vec{R}_2}\rangle}{\sqrt{2(1-\delta)}}, \quad |e_2\rangle = \frac{|\Psi_{\vec{R}_1}\rangle + e^{-ik(Z_1-Z_2)} |\Psi_{\vec{R}_2}\rangle}{\sqrt{2(1+\delta)}}, \quad (S4)$$

and we need to find more eigenvectors that span the support of $\frac{\partial |e_1\rangle}{\partial \lambda_\mu}$ and $\frac{\partial |e_2\rangle}{\partial \lambda_\mu}$.

Taking into account the form of the point spread function given by Eq. (2) in the main text, we can choose the following orthonormal set to complete the eigenbasis,

$$\begin{aligned} |e_3\rangle &= \frac{1}{\sqrt{c_3}} \left[|\Psi_{\vec{R}_1}\rangle_{X_1} + A |\Psi_{\vec{R}_2}\rangle_{X_2} + \frac{(1 + e^{ik(Z_1-Z_2)} A) \gamma}{\sqrt{2(1-\delta)}} |e_1\rangle - \frac{(1 - e^{ik(Z_1-Z_2)} A) \gamma}{\sqrt{2(1+\delta)}} |e_2\rangle \right], \\ |e_4\rangle &= \frac{1}{\sqrt{c_4}} \left[|\Psi_{\vec{R}_1}\rangle_{X_1} - A^* |\Psi_{\vec{R}_2}\rangle_{X_2} + \frac{(1 - e^{ik(Z_1-Z_2)} A^*) \gamma}{\sqrt{2(1-\delta)}} |e_1\rangle - \frac{(1 + e^{ik(Z_1-Z_2)} A^*) \gamma}{\sqrt{2(1+\delta)}} |e_2\rangle \right], \\ |e_5\rangle &= \frac{1}{\sqrt{c_5}} \left[|\Psi_{\vec{R}_1}\rangle_{Z_1} + R |\Psi_{\vec{R}_2}\rangle_{Z_2} + \frac{\Gamma_{12} - e^{ik(Z_1-Z_2)} R \Gamma_{21}}{\sqrt{2(1-\delta)}} |e_1\rangle - \frac{\Gamma_{12} + e^{ik(Z_1-Z_2)} R \Gamma_{21}}{\sqrt{2(1+\delta)}} |e_2\rangle \right. \\ &\quad + \frac{\gamma (\Gamma_{12} - A^* R \Gamma_{21}) - e^{ik(Z_1-Z_2)} R (\gamma \Gamma_{21} \delta + h_{X_1 Z_2} (1 - \delta^2)) + e^{-ik(Z_1-Z_2)} A^* (\gamma \Gamma_{12} \delta - h_{Z_1 X_2} (1 - \delta^2))}{\sqrt{c_3} (1 - \delta^2)} |e_3\rangle \\ &\quad \left. + \frac{\gamma (\Gamma_{12} + A R \Gamma_{21}) - e^{ik(Z_1-Z_2)} R (\gamma \Gamma_{21} \delta + h_{X_1 Z_2} (1 - \delta^2)) - e^{-ik(Z_1-Z_2)} A (\gamma \Gamma_{12} \delta - h_{Z_1 X_2} (1 - \delta^2))}{\sqrt{c_4} (1 - \delta^2)} |e_4\rangle \right], \\ |e_6\rangle &= \frac{1}{\sqrt{c_6}} \left[|\Psi_{\vec{R}_1}\rangle_{Z_1} - R^* |\Psi_{\vec{R}_2}\rangle_{Z_2} + \frac{\Gamma_{12} + e^{ik(Z_1-Z_2)} R^* \Gamma_{21}}{\sqrt{2(1-\delta)}} |e_1\rangle - \frac{\Gamma_{12} - e^{ik(Z_1-Z_2)} R^* \Gamma_{21}}{\sqrt{2(1+\delta)}} |e_2\rangle \right. \\ &\quad + \frac{\gamma (\Gamma_{12} - A^* R^* \Gamma_{21}) + e^{ik(Z_1-Z_2)} R^* (\gamma \Gamma_{21} \delta + h_{X_1 Z_2} (1 - \delta^2)) + e^{-ik(Z_1-Z_2)} A^* (\gamma \Gamma_{12} \delta - h_{Z_1 X_2} (1 - \delta^2))}{\sqrt{c_3} (1 - \delta^2)} |e_3\rangle \\ &\quad \left. + \frac{\gamma (\Gamma_{12} + A R^* \Gamma_{21}) + e^{ik(Z_1-Z_2)} R^* (\gamma \Gamma_{21} \delta + h_{X_1 Z_2} (1 - \delta^2)) - e^{-ik(Z_1-Z_2)} A (\gamma \Gamma_{12} \delta - h_{Z_1 X_2} (1 - \delta^2))}{\sqrt{c_4} (1 - \delta^2)} |e_4\rangle \right], \end{aligned} \quad (S5)$$

where

$$h_{X_1 Z_2} = \int_{-\infty}^{\infty} \left[\frac{\partial \psi_{Z_1}(x - X_1)}{\partial X_1} \right] \left[\frac{\partial \psi_{Z_2}(x - X_2)}{\partial Z_2} \right] dx,$$

$$h_{Z_1 X_2} = \int_{-\infty}^{\infty} \left[\frac{\partial \psi_{Z_1}(x - X_1)}{\partial Z_1} \right] \left[\frac{\partial \psi_{Z_2}(x - X_2)}{\partial X_2} \right] dx,$$

and A and R are two factors that make the vectors mutually orthogonal (their explicit expression is omitted here), while c_3 , c_4 , c_5 and c_6 are the normalization factors, and $\delta, \gamma, \Gamma_{12}, \Gamma_{21}$ are defined in the main text. The eigenvalues of ρ_1 are simply

$$\begin{aligned} d_1 &= \frac{1 - \delta}{2}, & d_2 &= \frac{1 + \delta}{2}, \\ d_3 &= 0, & d_4 &= 0, \\ d_5 &= 0, & d_6 &= 0. \end{aligned}$$

From this point, with some tedious algebra calculations, the derivatives (S3) can be evaluated and the SLD (S2) can be computed with respect to the source coordinates $(X_r, Z_r)_{r=1,2}$, and finally transformed in terms of the angular and axial separations and centroid coordinates, s, c, p, z , specified by Eq. (4) in the main text. Explicitly, we find that the SLDs take the following expression:

$$L_s = \begin{pmatrix} \frac{\gamma}{1-\delta} & 0 & -\frac{\sqrt{c_3}(e^{ik(Z_1-Z_2)}+A)}{(A+A^*)\sqrt{2(1-\delta)}} & \frac{\sqrt{c_4}(e^{ik(Z_1-Z_2)}-A^*)}{(A+A^*)\sqrt{2(1-\delta)}} & 0 & 0 \\ 0 & -\frac{\gamma}{1+\delta} & \frac{\sqrt{c_3}(e^{-ik(Z_1-Z_2)}-A^*)}{(A+A^*)\sqrt{2(1-\delta)}} & -\frac{\sqrt{c_4}(e^{ik(Z_1-Z_2)}+A^*)}{(A+A^*)\sqrt{2(1+\delta)}} & 0 & 0 \\ -\frac{\sqrt{c_3}(e^{-ik(Z_1-Z_2)}+A^*)}{(A+A^*)\sqrt{2(1-\delta)}} & \frac{\sqrt{c_3}(e^{-ik(Z_1-Z_2)}-A^*)}{(A+A^*)\sqrt{2(1-\delta)}} & 0 & 0 & 0 & 0 \\ \frac{\sqrt{c_4}(e^{-ik(Z_1-Z_2)}-A)}{(A+A^*)\sqrt{2(1-\delta)}} & -\frac{\sqrt{c_4}(e^{-ik(Z_1-Z_2)}+A)}{(A+A^*)\sqrt{2(1+\delta)}} & 0 & 0 & 0 & 0 \\ 0 & 0 & 0 & 0 & 0 & 0 \\ 0 & 0 & 0 & 0 & 0 & 0 \end{pmatrix},$$

$$L_c = \begin{pmatrix} 0 & -\frac{2\gamma\delta}{\sqrt{1-\delta^2}} & -\frac{\sqrt{2c_3}(e^{ik(Z_1-Z_2)}-A)}{(A+A^*)\sqrt{1-\delta}} & \frac{\sqrt{2c_4}(e^{ik(Z_1-Z_2)}+A^*)}{(A+A^*)\sqrt{1-\delta}} & 0 & 0 \\ -\frac{2\gamma\delta}{\sqrt{1-\delta^2}} & 0 & \frac{\sqrt{2c_3}(e^{ik(Z_1-Z_2)}+A)}{(A+A^*)\sqrt{1+\delta}} & -\frac{\sqrt{2c_4}(e^{ik(Z_1-Z_2)}-A^*)}{(A+A^*)\sqrt{1+\delta}} & 0 & 0 \\ -\frac{\sqrt{2c_3}(e^{-ik(Z_1-Z_2)}-A^*)}{(A+A^*)\sqrt{1-\delta}} & \frac{\sqrt{2c_3}(e^{-ik(Z_1-Z_2)}+A^*)}{(A+A^*)\sqrt{1+\delta}} & 0 & 0 & 0 & 0 \\ \frac{\sqrt{2c_4}(e^{-ik(Z_1-Z_2)}+A)}{(A+A^*)\sqrt{1-\delta}} & -\frac{\sqrt{2c_4}(e^{-ik(Z_1-Z_2)}-A)}{(A+A^*)\sqrt{1+\delta}} & 0 & 0 & 0 & 0 \\ 0 & 0 & 0 & 0 & 0 & 0 \\ 0 & 0 & 0 & 0 & 0 & 0 \end{pmatrix},$$

$$\begin{aligned}
L_{p1,1} &= \frac{\Gamma_{12} - \Gamma_{21} + \delta_{Z_1} + \delta_{Z_2}}{2(1 - \delta)}, & L_{p1,2} &= \frac{(\Gamma_{12} + \Gamma_{21})\delta}{2\sqrt{1 - \delta^2}}, \\
L_{p1,3} &= \frac{\gamma(\Gamma_{12} - \Gamma_{21}\delta) - h_{X_1Z_2}(1 - \delta^2) + Ae^{ik(Z_1 - Z_2)}(\gamma(\Gamma_{12}\delta - \Gamma_{21}) - h_{X_2Z_1}(1 - \delta^2))}{\sqrt{c_3}\sqrt{2(1 - \delta)}(1 - \delta^2)}, \\
L_{p1,4} &= \frac{\gamma(\Gamma_{12} - \Gamma_{21}\delta) - h_{X_1Z_2}(1 - \delta^2) - A^*e^{ik(Z_1 - Z_2)}(\gamma(\Gamma_{12}\delta - \Gamma_{21}) - h_{X_2Z_1}(1 - \delta^2))}{\sqrt{c_4}\sqrt{2(1 - \delta)}(1 - \delta^2)}, \\
L_{p1,5} &= -\frac{\sqrt{c_5}(e^{ik(Z_1 - Z_2)} + R)}{(R + R^*)\sqrt{2(1 - \delta)}}, & L_{p1,6} &= \frac{\sqrt{c_6}(e^{ik(Z_1 - Z_2)} - R^*)}{(R + R^*)\sqrt{2(1 - \delta)}}, \\
L_{p2,1} &= \frac{(\Gamma_{12} + \Gamma_{21})\delta}{2\sqrt{1 - \delta^2}}, & L_{p2,2} &= -\frac{\Gamma_{12} - \Gamma_{21} - \delta_{Z_1} - \delta_{Z_2}}{2(1 + \delta)}, \\
L_{p2,3} &= \frac{\gamma(\Gamma_{12} + \Gamma_{21}\delta) + h_{X_1Z_2}(1 - \delta^2) + Ae^{ik(Z_1 - Z_2)}(\gamma(\Gamma_{12}\delta + \Gamma_{21}) - h_{X_2Z_1}(1 - \delta^2))}{\sqrt{c_3}\sqrt{2(1 + \delta)}(1 - \delta^2)}, \\
L_{p2,4} &= \frac{\gamma(\Gamma_{12} + \Gamma_{21}\delta) + h_{X_1Z_2}(1 - \delta^2) - A^*e^{ik(Z_1 - Z_2)}(\gamma(\Gamma_{12}\delta + \Gamma_{21}) - h_{X_2Z_1}(1 - \delta^2))}{\sqrt{c_4}\sqrt{2(1 + \delta)}(1 - \delta^2)}, \\
L_{p2,5} &= \frac{\sqrt{c_5}(e^{ik(Z_1 - Z_2)} - R)}{(R + R^*)\sqrt{2(1 + \delta)}}, & L_{p2,6} &= -\frac{\sqrt{c_6}(e^{ik(Z_1 - Z_2)} + R^*)}{(R + R^*)\sqrt{2(1 + \delta)}}, \\
L_{p3,1} &= \frac{\gamma(\Gamma_{12} - \Gamma_{21}\delta) - h_{X_1Z_2}(1 - \delta^2) + A^*e^{-ik(Z_1 - Z_2)}(\gamma(\Gamma_{12}\delta - \Gamma_{21}) - h_{X_2Z_1}(1 - \delta^2))}{\sqrt{c_3}\sqrt{2(1 - \delta)}(1 - \delta^2)}, \\
L_{p3,2} &= \frac{\gamma(\Gamma_{12} + \Gamma_{21}\delta) + h_{X_1Z_2}(1 - \delta^2) + A^*e^{-ik(Z_1 - Z_2)}(\gamma(\Gamma_{12}\delta + \Gamma_{21}) - h_{X_2Z_1}(1 - \delta^2))}{\sqrt{c_3}\sqrt{2(1 + \delta)}(1 - \delta^2)}, \\
L_{p3,3} &= 0, & L_{p3,4} &= 0, & L_{p3,5} &= 0, & L_{p3,6} &= 0, \\
L_{p4,1} &= \frac{\gamma(\Gamma_{12} - \Gamma_{21}\delta) - h_{X_1Z_2}(1 - \delta^2) - Ae^{-ik(Z_1 - Z_2)}(\gamma(\Gamma_{12}\delta - \Gamma_{21}) - h_{X_2Z_1}(1 - \delta^2))}{\sqrt{c_4}\sqrt{2(1 - \delta)}(1 - \delta^2)}, \\
L_{p4,2} &= \frac{\gamma(\Gamma_{12} + \Gamma_{21}\delta) + h_{X_1Z_2}(1 - \delta^2) - Ae^{-ik(Z_1 - Z_2)}(\gamma(\Gamma_{12}\delta + \Gamma_{21}) - h_{X_2Z_1}(1 - \delta^2))}{\sqrt{c_4}\sqrt{2(1 + \delta)}(1 - \delta^2)}, \\
L_{p4,3} &= 0, & L_{p4,4} &= 0, & L_{p4,5} &= 0, & L_{p4,6} &= 0, \\
L_{p5,1} &= -\frac{\sqrt{c_5}(e^{-ik(Z_1 - Z_2)} + R^*)}{(R + R^*)\sqrt{2(1 - \delta)}}, & L_{p5,2} &= \frac{\sqrt{c_5}(e^{-ik(Z_1 - Z_2)} - R^*)}{(R + R^*)\sqrt{2(1 + \delta)}}, \\
L_{p5,3} &= 0, & L_{p5,4} &= 0, & L_{p5,5} &= 0, & L_{p5,6} &= 0, \\
L_{p6,1} &= \frac{\sqrt{c_6}(e^{-ik(Z_1 - Z_2)} - R)}{(R + R^*)\sqrt{2(1 - \delta)}}, & L_{p6,2} &= -\frac{\sqrt{c_6}(e^{-ik(Z_1 - Z_2)} + R)}{(R + R^*)\sqrt{2(1 + \delta)}}, \\
L_{p6,3} &= 0, & L_{p6,4} &= 0, & L_{p6,5} &= 0, & L_{p6,6} &= 0,
\end{aligned}$$

$$\begin{aligned}
L_{z1,1} &= -\frac{\Gamma_{12} - \Gamma_{21} - \delta_{Z_1} - \delta_{Z_2}}{(1 - \delta)}, & L_{z1,2} &= -\frac{(\Gamma_{12} - \Gamma_{21})\delta}{\sqrt{1 - \delta^2}}, \\
L_{z1,3} &= -\frac{\sqrt{2}(\gamma(\Gamma_{12} + \Gamma_{21}\delta) + h_{X_1Z_2}(1 - \delta^2) + Ae^{ik(Z_1-Z_2)}(\gamma(\Gamma_{12}\delta + \Gamma_{21}) - h_{X_2Z_1}(1 - \delta^2)))}{\sqrt{c_3}\sqrt{1 - \delta}(1 - \delta^2)}, \\
L_{z1,4} &= \frac{\sqrt{2}(\gamma(\Gamma_{12} + \Gamma_{21}\delta) + h_{X_1Z_2}(1 - \delta^2) - A^*e^{ik(Z_1-Z_2)}(\gamma(\Gamma_{12}\delta + \Gamma_{21}) - h_{X_2Z_1}(1 - \delta^2)))}{\sqrt{c_4}\sqrt{1 - \delta}(1 - \delta^2)}, \\
L_{z1,5} &= -\frac{\sqrt{2c_5}(e^{ik(Z_1-Z_2)} - R)}{(R + R^*)\sqrt{1 - \delta}}, & L_{z1,6} &= -\frac{\sqrt{2c_6}(e^{ik(Z_1-Z_2)} + R^*)}{(R + R^*)\sqrt{1 - \delta}}, \\
L_{z2,1} &= -\frac{(\Gamma_{12} - \Gamma_{21})\delta}{\sqrt{1 - \delta^2}}, & L_{z2,2} &= \frac{\Gamma_{12} + \Gamma_{21} - \delta_{Z_1} - \delta_{Z_2}}{(1 + \delta)}, \\
L_{z2,3} &= -\frac{\sqrt{2}(\gamma(\Gamma_{12} - \Gamma_{21}\delta) - h_{X_1Z_2}(1 - \delta^2) + Ae^{ik(Z_1-Z_2)}(\gamma(\Gamma_{12}\delta - \Gamma_{21}) - h_{X_2Z_1}(1 - \delta^2)))}{\sqrt{c_3}\sqrt{1 + \delta}(1 - \delta^2)}, \\
L_{z2,4} &= -\frac{\sqrt{2}(\gamma(\Gamma_{12} - \Gamma_{21}\delta) - h_{X_1Z_2}(1 - \delta^2) + A^*e^{ik(Z_1-Z_2)}(\gamma(\Gamma_{12}\delta - \Gamma_{21}) + h_{X_2Z_1}(1 - \delta^2)))}{\sqrt{c_4}\sqrt{1 + \delta}(1 - \delta^2)}, \\
L_{z2,5} &= \frac{\sqrt{2c_5}(e^{ik(Z_1-Z_2)} + R)}{(R + R^*)\sqrt{1 + \delta}}, & L_{z2,6} &= -\frac{\sqrt{2c_6}(e^{ik(Z_1-Z_2)} - R^*)}{(R + R^*)\sqrt{1 + \delta}}, \\
L_{z3,1} &= -\frac{\sqrt{2}(\gamma(\Gamma_{12} + \Gamma_{21}\delta) + h_{X_1Z_2}(1 - \delta^2) + A^*e^{-ik(Z_1-Z_2)}(\gamma(\Gamma_{12}\delta + \Gamma_{21}) - h_{X_2Z_1}(1 - \delta^2)))}{\sqrt{c_3}\sqrt{1 - \delta}(1 - \delta^2)}, \\
L_{z3,2} &= -\frac{\sqrt{2}(\gamma(\Gamma_{12} - \Gamma_{21}\delta) - h_{X_1Z_2}(1 - \delta^2) + A^*e^{-ik(Z_1-Z_2)}(\gamma(\Gamma_{12}\delta - \Gamma_{21}) - h_{X_2Z_1}(1 - \delta^2)))}{\sqrt{c_3}\sqrt{1 + \delta}(1 - \delta^2)}, \\
L_{z3,3} &= 0, & L_{z3,4} &= 0, & L_{z3,5} &= 0, & L_{z3,6} &= 0, \\
L_{z4,1} &= \frac{\sqrt{2}(\gamma(\Gamma_{12} + \Gamma_{21}\delta) + h_{X_1Z_2}(1 - \delta^2) - Ae^{-ik(Z_1-Z_2)}(\gamma(\Gamma_{12}\delta + \Gamma_{21}) - h_{X_2Z_1}(1 - \delta^2)))}{\sqrt{c_4}\sqrt{1 - \delta}(1 - \delta^2)}, \\
L_{z4,2} &= -\frac{\sqrt{2}(\gamma(\Gamma_{12} - \Gamma_{21}\delta) - h_{X_1Z_2}(1 - \delta^2) + Ae^{-ik(Z_1-Z_2)}(\gamma(\Gamma_{12}\delta - \Gamma_{21}) + h_{X_2Z_1}(1 - \delta^2)))}{\sqrt{c_4}\sqrt{1 + \delta}(1 - \delta^2)}, \\
L_{z4,3} &= 0, & L_{z4,4} &= 0, & L_{z4,5} &= 0, & L_{z4,6} &= 0, \\
L_{z5,1} &= -\frac{\sqrt{2c_5}(e^{-ik(Z_1-Z_2)} - R^*)}{(R + R^*)\sqrt{1 - \delta}}, & L_{z5,2} &= \frac{\sqrt{2c_5}(e^{-ik(Z_1-Z_2)} + R^*)}{(R + R^*)\sqrt{1 + \delta}}, \\
L_{z5,3} &= 0, & L_{z5,4} &= 0, & L_{z5,5} &= 0, & L_{z5,6} &= 0, \\
L_{z6,1} &= \frac{\sqrt{2c_6}(e^{-ik(Z_1-Z_2)} + R)}{(R + R^*)\sqrt{1 - \delta}}, & L_{z6,2} &= -\frac{\sqrt{2c_6}(e^{-ik(Z_1-Z_2)} - R)}{(R + R^*)\sqrt{1 + \delta}}, \\
L_{z6,3} &= 0, & L_{z6,4} &= 0, & L_{z6,5} &= 0, & L_{z6,6} &= 0.
\end{aligned}$$

We can now substitute the SLDs into Eq. (6) to compute the qFim H .
The final result is given by Eqs. (8) and (9) in the main text.

Appendix B: Verification of the measurement compatibility condition

As we mentioned in the main text, the multiparameter Cramér-Rao bound (qCRb), Eq. (5), is not always achievable if the SLDs L_μ corresponding to different parameters do not commute. However, a necessary and sufficient condition to saturate the bound asymptotically is that the SLDs corresponding to different parameters commute on average on the probe state,

$$\text{Tr}(\rho_1 [L_\mu, L_\nu]) = 0, \quad \forall \mu \neq \nu. \quad (\text{S6})$$

Taking in account the SLDs reported in Appendix A, it is easy to show that this condition is always satisfied for any point spread function compliant with Eq. (2). Explicitly, given the state

$$\rho_1 = \begin{pmatrix} \frac{1-\delta}{2} & 0 & 0 & 0 & 0 & 0 \\ 0 & \frac{1+\delta}{2} & 0 & 0 & 0 & 0 \\ 0 & 0 & 0 & 0 & 0 & 0 \\ 0 & 0 & 0 & 0 & 0 & 0 \\ 0 & 0 & 0 & 0 & 0 & 0 \\ 0 & 0 & 0 & 0 & 0 & 0 \end{pmatrix}, \quad (\text{S7})$$

the diagonal elements of $(\rho_1 [L_\mu, L_\nu])$ for all $\mu \neq \nu$ are

$$\begin{aligned} \text{diag}\{\rho_1 [L_s, L_c]\} = & \text{diag}\left\{ \frac{(c_3 A - c_4 A^*) e^{-ik(Z_1 - Z_2)} - (c_3 A^* - c_4 A) e^{ik(Z_1 - Z_2)}}{(A + A^*)^2}, \right. \\ & \left. - \frac{(c_3 A - c_4 A^*) e^{-ik(Z_1 - Z_2)} - (c_3 A^* - c_4 A) e^{ik(Z_1 - Z_2)}}{(A + A^*)^2}, 0, 0, 0, 0 \right\}, \end{aligned}$$

$$\text{diag}\{\rho_1 [L_s, L_c]\} = \text{diag}\{y_{sc}, -y_{sc}, 0, 0, 0, 0\},$$

$$\text{diag}\{\rho_1 [L_s, L_p]\} = \text{diag}\{0, 0, 0, 0, 0, 0\},$$

$$\text{diag}\{\rho_1 [L_s, L_z]\} = \text{diag}\{0, 0, 0, 0, 0, 0\},$$

$$\text{diag}\{\rho_1 [L_c, L_p]\} = \text{diag}\{0, 0, 0, 0, 0, 0\},$$

$$\text{diag}\{\rho_1 [L_c, L_z]\} = \text{diag}\{0, 0, 0, 0, 0, 0\},$$

$$\text{diag}\{\rho_1 [L_p, L_z]\} = \text{diag}\{y_{pz}, -y_{pz}, 0, 0, 0, 0\},$$

with

$$\begin{aligned} y_{sc} &= \frac{(c_3 A - c_4 A^*) e^{-ik(Z_1 - Z_2)} - (c_3 A^* - c_4 A) e^{ik(Z_1 - Z_2)}}{(A + A^*)^2}, \\ y_{pz} &= \frac{(c_5 R - c_6 R^*) e^{-ik(Z_1 - Z_2)} - (c_5 R^* - c_6 R) e^{ik(Z_1 - Z_2)}}{(R + R^*)^2} + \left(\frac{\gamma (\gamma \Gamma_{12} \Gamma_{21} - \delta (\Gamma_{12} h_{X_1 Z_2} - \Gamma_{21} h_{X_2 Z_1}))}{1 - \delta^2} + h_{X_1 Z_2} h_{X_2 Z_1} \right) \frac{(A + A^*)^2 y_{sc}}{c_3 c_4} \end{aligned}$$

From here, it is immediate to verify that the measurement compatibility condition given by Eq. (S6) is fulfilled.